Fast skeletal myosin-binding protein-C regulates fast skeletal muscle contraction

Taejeong Song[a], James W. McNamara[a,1,2], Weikang Ma[b], Maicon Landim-Vieira[c], Kyoung Hwan Lee[d,3], Lisa A. Martin[a], Judith A. Heiny[e], John N. Lorenz[e], Roger Craig[d], Jose Renato Pinto[c], Thomas Irving[b], and Sakthivel Sadayappan[a,4]

[a]Division of Cardiovascular Health and Disease, Department of Internal Medicine, University of Cincinnati, OH 45267; [b]Biophysics Collaborative Access Team, Department of Biological Sciences, Illinois Institute of Technology, Chicago, IL 60616; [c]Department of Biomedical Sciences, Florida State University College of Medicine, Tallahassee, FL 32306; [d]Division of Cell Biology and Imaging, Department of Radiology, University of Massachusetts Medical School, Worcester, MA 01655; and [e]Department of Pharmacology and Systems Physiology, University of Cincinnati College of Medicine, Cincinnati, OH 45267

Edited by Jonathan Seidman, Harvard University, Boston, MA, and approved March 19, 2021 (received for review February 25, 2020)

Fast skeletal myosin-binding protein-C (fMyBP-C) is one of three MyBP-C paralogs and is predominantly expressed in fast skeletal muscle. Mutations in the gene that encodes fMyBP-C, *MYBPC2*, are associated with distal arthrogryposis, while loss of fMyBP-C protein is associated with diseased muscle. However, the functional and structural roles of fMyBP-C in skeletal muscle remain unclear. To address this gap, we generated a homozygous fMyBP-C knockout mouse ($C2^{-/-}$) and characterized it both in vivo and in vitro compared to wild-type mice. Ablation of fMyBP-C was benign in terms of muscle weight, fiber type, cross-sectional area, and sarcomere ultrastructure. However, grip strength and plantar flexor muscle strength were significantly decreased in $C2^{-/-}$ mice. Peak isometric tetanic force and isotonic speed of contraction were significantly reduced in isolated extensor digitorum longus (EDL) from $C2^{-/-}$ mice. Small-angle X-ray diffraction of $C2^{-/-}$ EDL muscle showed significantly increased equatorial intensity ratio during contraction, indicating a greater shift of myosin heads toward actin, while MLL4 layer line intensity was decreased at rest, indicating less ordered myosin heads. Interfilament lattice spacing increased significantly in $C2^{-/-}$ EDL muscle. Consistent with these findings, we observed a significant reduction of steady-state isometric force during Ca^{2+}-activation, decreased myofilament calcium sensitivity, and sinusoidal stiffness in skinned EDL muscle fibers from $C2^{-/-}$ mice. Finally, $C2^{-/-}$ muscles displayed disruption of inflammatory and regenerative pathways, along with increased muscle damage upon mechanical overload. Together, our data suggest that fMyBP-C is essential for maximal speed and force of contraction, sarcomere integrity, and calcium sensitivity in fast-twitch muscle.

MYBPC2 | fMyBP-C | skeletal muscle | distal arthrogryposis | contraction

Myosin-binding protein-C (MyBP-C) is a thick filament-associated protein expressed in striated muscle. Initially discovered in skeletal muscle (1), three paralogs of MyBP-C, encoded by different genes, have been described: slow skeletal (sMyBP-C), fast skeletal (fMyBP-C), and cardiac MyBP-C (cMyBP-C) (2). The paralogs share a conserved domain structure that consists of seven immunoglobulin (Ig), three fibronectin type 3 (FN3), proline/alanine-rich, and M domains. All paralogs localize to the C-zone within the A-band region at a periodicity of 43 nm, corresponding to the position of unlabeled native stripes (3). C-terminal regions (C8 to C10) of MyBP-C anchor it to the light meromyosin of myosin and titin, while its N terminus interacts with actin and myosin subfragment 2 (4). The importance of sMyBP-C and cMyBP-C in muscle physiology has been previously established by their structural and regulatory roles within the sarcomere, extending beyond simply regulating contractility via modulation of actin and myosin interactions. However, the roles of fMyBP-C are less clear (5, 6).

Over the last two decades, the pathophysiological function of cMyBP-C in cardiac muscle has been widely studied owing to its role in familial forms of hypertrophic cardiomyopathy (7, 8). Studies on cardiac papillary muscle indicate differences in functional responses to $[Ca^{2+}]$ among MyBP-C paralogs, a likely result of distinct effects on thin filament activation (9). Interest in understanding the functional roles of sMyBP-C and fMyBP-C in skeletal muscle is growing, in particular after their recent association with the development of congenital skeletal muscle diseases, including distal arthrogryposis and lethal congenital contracture syndrome 4 (10, 11). sMyBP-C is the more ubiquitous of the two paralogs and is expressed primarily in both fast and slow-twitch muscle and at low levels in atrial tissue (12). Additionally, splice variants have been described in human and mouse skeletal muscles (13, 14). In contrast, fMyBP-C has not been well studied, and its structural and functional roles in skeletal muscle remain to be elucidated. The fMyBP-C paralog is highly expressed in fast-twitch muscle (14); however, its exact expression profile has remained unclear. Intriguingly, up-regulation of its expression has been documented

Significance

Myosin-binding protein-C (MyBP-C) is a thick filament regulatory protein found exclusively in the C-zone of the A-band in the sarcomeres of vertebrate striated muscle. Cardiac, slow skeletal, and fast skeletal MyBP-C (fMyBP-C) paralogs perform different functions. All three paralogs share similar protein structures but likely differ substantially in terms of expression and function, which may serve the distinct physiologies of fast and slow muscle fibers. However, the functional role of fMyBP-C in fast skeletal muscle is completely unknown. Genetic mutations in human fMyBP-C lead to skeletal myopathies. In this study, we used knockout mice to define the molecular basis for fMyBP-C paralog diversity. We demonstrate that fMyBP-C modulates the speed and force of fast skeletal muscle contraction.

Author contributions: T.S., J.W.M., W.M., M.L.-V., K.H.L., J.A.H., R.C., J.R.P., T.I., and S.S. designed research; T.S., J.W.M., W.M., M.L.-V., K.H.L., J.R.P., T.I., and S.S. performed research; T.S., J.W.M., W.M., M.L.-V., K.H.L., L.A.M., J.A.H., J.N.L., R.C., J.R.P., T.I., and S.S. contributed new reagents/analytic tools; T.S., J.W.M., W.M., M.L.-V., K.H.L., J.A.H., J.N.L., R.C., J.R.P., T.I., and S.S. analyzed data; and T.S., J.W.M., W.M., M.L.-V., K.H.L., L.A.M., J.A.H., J.N.L., R.C., J.R.P., T.I., and S.S. wrote the paper.

Competing interest statement: S.S. provided consulting and collaborative research studies to the Leducq Foundation, Red Saree Inc., Greater Cincinnati Tamil Sangam, AstraZeneca, MyoKardia, Merck, and Amgen, but such work is unrelated to the content of this manuscript.

This article is a PNAS Direct Submission.

[1]Present address: Murdoch Children's Research Institute, The Royal Children's Hospital, Parkville VIC 3052, Australia.

[2]Present address: Department of Physiology, School of Biomedical Sciences, The University of Melbourne, Parkville VIC 3010, Australia.

[3]Present address: Massachusetts Facility for High-Resolution Electron Cryo-Microscopy, University of Massachusetts Medical School, Worcester, MA 01655.

[4]To whom correspondence may be addressed. Email: sadayasl@ucmail.uc.edu.

This article contains supporting information online at https://www.pnas.org/lookup/suppl/doi:10.1073/pnas.2003596118/-/DCSupplemental.

Published April 22, 2021.

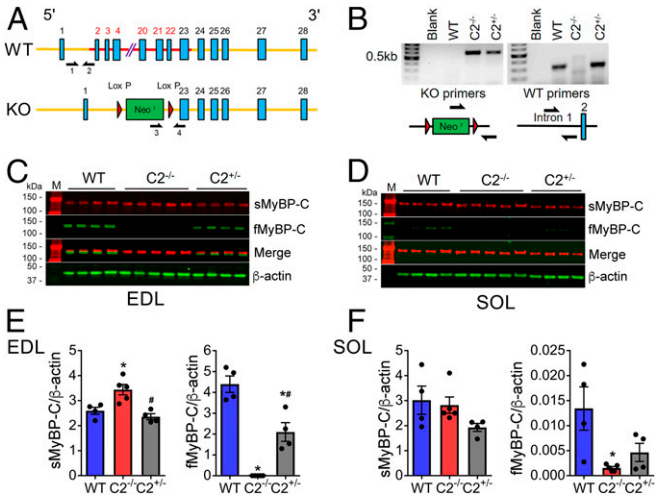

Fig. 1. fMyBP-C KO increases the level of sMyBP-C expression in $C2^{-/-}$ muscles. (*A*) Schematic illustration of *Mybpc2* gene KO in mouse chromosome 7. (*B*) Genotype of WT, homozygous ($C2^{-/-}$), and heterozygous ($C2^{+/-}$) mice was determined by PCR to detect KO and WT alleles. Protein expression of sMyBP-C and fMyBP-C was measured in (*C*) EDL and (*D*) SOL muscles of WT, $C2^{-/-}$, and $C2^{+/-}$ mice by Western blot. A molecular weight marker labeled M was loaded on both sides of the gel. The quantification of protein expression of sMyBP-C and fMyBP-C in (*E*) EDL and (*F*) SOL of WT, $C2^{-/-}$, and $C2^{+/-}$ mice ($n = 4$ to 5 in each group). Error bars represent ± SEM, $^{*}P < 0.05$ to WT and $^{\#}P < 0.05$ to $C2^{-/-}$. Statistical analyses were performed in all groups by ordinary one-way ANOVA followed by Tukey's multiple comparison test.

in failing murine hearts, suggesting that it may play a role in functional compensation (14). In a murine model of denervation-induced muscle atrophy, fMyBP-C was found to be degraded, along with myosin light chains, via a MuRF1-dependent mechanism (15). Knockdown of >50% fMyBP-C expression in zebrafish by morpholino antisense nucleotides led to the development of significant skeletal muscle atrophy and functional deficits concomitant with elevated expression of atrophy-related genes (6). However, the specific physiological roles of fMyBP-C in mammalian skeletal muscle remain unknown.

In the present study, we developed a fMyBP-C global knockout (KO) mouse model ($C2^{-/-}$) to investigate the structural, functional, and physiological roles of fMyBP-C in skeletal muscle. Both in vitro and in vivo studies reveal that fMyBP-C modulates myofilament calcium sensitivity and fine-tunes actin–myosin interactions to match force production to the demands of fast-twitch skeletal muscles. In summary, our studies provide evidence that fMyBP-C regulates force, power, and contractile speed in fast-twitch muscles.

Results

fMyBP-C Ablation in Mice Does Not Cause Major Disruptions in Development. Genetic deletion of fMyBP-C ($C2^{-/-}$) was achieved by the replacement of exons 2 to 22 of the *Mybpc2* gene with a neomycin cassette (Fig. 1 *A* and *B*). Homozygous $C2^{-/-}$ mice displayed a complete KO of fMyBP-C in both fast-type extensor digitorum longus (EDL) and slow-type soleus (SOL) skeletal muscles, compared to heterozygous ($C2^{+/-}$) and wild-type (WT) controls (Fig. 1 *C–F*). As previously reported (14), fMyBP-C expression in SOL was extremely low in WT but completely ablated in $C2^{-/-}$ (Fig. 1 *D* and *F*). Interestingly, $C2^{-/-}$ elicited 33% higher expression of sMyBP-C in EDL but not in SOL muscles (Fig. 1 *C–F*). However, $C2^{-/-}$ mice showed no gross changes in body weight and appearance, and no differences were noted in cardiac function (*SI Appendix*, Table S1) or cardiac and hindlimb muscle mass between WT and $C2^{-/-}$ mouse groups (*SI Appendix*, Table S2) with no obvious increases in morbidity and mortality.

fMyBP-C KO Results in Reduced Force Generation and Contraction Speed In Vivo. To uncover the functional role of fMyBP-C in skeletal muscle, we compared in vivo muscle performance between WT and $C2^{-/-}$ mice. Maximum grip strength (Table 1) and treadmill running times (*SI Appendix*, Fig. S1*A*) were significantly reduced in $C2^{-/-}$ mice compared to WT. Plantar flexor muscle strength, measured as maximum isometric tetanic force, was significantly reduced in $C2^{-/-}$ compared to WT (*SI Appendix*, Fig. S1*B*). The functional role of fMyBP-C was next evaluated in isolated intact EDL (fast-) and SOL (slow-type) muscles. In $C2^{-/-}$ EDL, peak isometric tetanic force (P_o) and specific force (SP_o) were significantly decreased compared to WT (Table 1). Force–frequency analysis indicated that the isometric tetanic force of $C2^{-/-}$ EDL was significantly lower at both maximal and submaximal stimulation frequencies (Fig. 2*A*). While no difference in the rate of contraction (+dF/dt) was observed (Fig. 2*B*), the rate of relaxation (−dF/dt) was significantly reduced in $C2^{-/-}$ EDL compared to WT over a range of stimulation frequencies (Fig. 2*C*). In SOL, however, P_o and SP_o were not significantly different between WT and $C2^{-/-}$ (*SI Appendix*, Fig. S2 *A–C*). Maximum isometric twitch force (P_t) of EDL and SOL was comparable in both genotypes (*SI Appendix*, Table S3). Next, measurements of isotonic speed of contraction were obtained in EDL and SOL muscles adjusted to optimal length (L_0) and maximally stimulated at 150 Hz at 10, 20, 40, 60, and 80% of each muscle's tetanic maximal force. The speed of EDL contraction was significantly slower in $C2^{-/-}$ at high relative force, 60 and 80% of P_o, compared to WT, while no differences in velocity were observed at lower relative forces (*SI Appendix*, Fig. S1*C*). Intact $C2^{-/-}$ EDL muscles generated significantly less power than WT controls (Fig. 2*D* and *SI Appendix*, Table S4). In SOL, however, isotonic speed of contraction was similar between WT and $C2^{-/-}$ at all ranges of applied tension (*SI Appendix*, Fig. S2*D*). This is consistent with the very low expression of fMyBP-C in SOL muscle (Fig. 1 *D–F*). Collectively, these in vivo and ex vivo measurements of contractile function indicate that fMyBP-C contributes to force generation, power output, and contraction speed at high loads in fast-twitch, but not slow-twitch, muscles.

fMyBP-C Is Predominantly Expressed in Type IIb Fibers, while KO Does Not Alter Muscle Structure. The expression profile of slow and fast MyBP-C in different fiber types may be related to differences in muscle function. To address this question, frozen EDL muscles were serially sectioned and immunostained with various myosin heavy chain (MHC) and skeletal MyBP-C antibodies. Interestingly, while fMyBP-C was expressed in type IIb and a few type IIx fibers (Fig. 3*A*), it was not detected in type I and type IIa fibers. In contrast, sMyBP-C was ubiquitously expressed across all fiber types (Fig. 3*A*). Therefore, fMyBP-C expression is mainly restricted to type IIb fast-twitch fibers. This expression profile of fMyBP-C was also validated by single-fiber Western blot analysis (*SI Appendix*, Fig. S3). The deletion of fMyBP-C slightly decreased the percentage

Table 1. Reduced grip strength and ex vivo EDL force generation in $C2^{-/-}$ at 3 mo of age

	GS/BW (mg/g)	P_o (mN)	SP_o (N/cm^2)
WT	7.77 ± 0.16	335 ± 14.21	23.98 ± 1.20
$C2^{+/-}$	7.52 ± 0.14	307 ± 19.61	22.97 ± 0.69
$C2^{-/-}$	7.12 ± 0.23*	276 ± 15.43*	19.53 ± 0.59**$^{\#}$

In addition to maximum grip strength (normalized to body weight [GS/BW] WT, $n = 11$; $C2^{+/-}$, $n = 11$; and $C2^{-/-}$, $n = 12$), the peak isometric tetanic force (P_o) and specific force (SP_o) of EDL muscle ($n = 4$ to 8 in each group) were significantly decreased in $C2^{-/-}$ groups. Both male and female mice were included for the analysis. The number in parentheses is SEM. $^{*}P < 0.05$ and $^{**}P < 0.01$ to WT, $^{\#}P < 0.05$ to $C2^{+/-}$. Statistical analyses were performed in all groups by one-way ANOVA followed by Tukey's multiple comparison test.

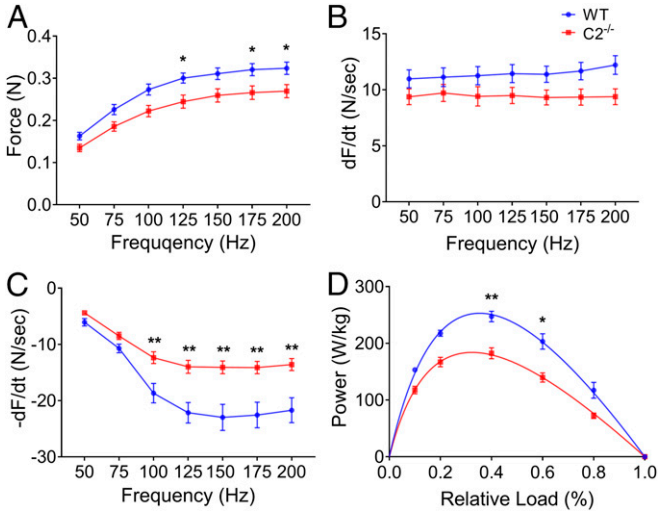

Fig. 2. Force–frequency relationship and isotonic power generation of WT and $C2^{-/-}$ EDL muscles. (*A*) Escalated isometric tetanic force generation over increasing electrical frequency (50 to 200 Hz at 50 mA). Rates of (*B*) force development and (*C*) relaxation are depicted at given frequency. (*D*) Power generation of EDL muscle during isotonic muscle contraction at specific relative force ($n = 5$ to 9 in each group). Error bars represent ± SEM and $*P < 0.05$ and $**P < 0.01$ versus WT. Statistical analyses were performed in all groups by unpaired *t* test or ordinary two-way ANOVA followed by Bonferroni's multiple comparison test.

of EDL type I fibers. However, since type I fibers comprise only 5% of fibers of this muscle, the overall distribution of other major fiber types remained unaltered (*SI Appendix*, Fig. S4*A*). In addition, the average cross-sectional area of each fiber type was similar between WT and $C2^{-/-}$ EDL muscle (*SI Appendix*, Fig. S4*B*). Therefore, deletion of fMyBP-C does not affect overall fiber type distribution or size.

Next, to determine whether $C2^{-/-}$ alters the spatial distribution and organization of sMyBP-C in the sarcomere (16), skinned EDL fibers were immunolabeled with sMyBP-C antibodies. Results showed that sMyBP-C localization, as a doublet pattern, was preserved in the C-zone between two Z-disks in the $C2^{-/-}$ sarcomere (Fig. 3*B*). The distribution of fluorescence signals and the distance between two peak signals of sMyBP-C in the sarcomere were unchanged in the $C2^{-/-}$ EDL fibers (Fig. 3*C* and *SI Appendix*, Fig. S5). By measuring the distance between two α-actinin bands (WT; 1.69 ± 0.02 μm versus $C2^{-/-}$; 1.74 ± 0.02 μm), we confirmed no difference in sarcomere length between WT and $C2^{-/-}$. The peak-to-peak distance of fMyBP-C was slightly shorter than that of sMyBP-C in WT EDL (648 ± 3 nm versus 684 ± 9 nm, $P < 0.01$) (Fig. 3 *C* and *D*). However, double immunostaining of sMyBP-C and fMyBP-C showed nearly complete overlap of these two paralogs (Fig. 3*B*). As expected, fMyBP-C was not detected in $C2^{-/-}$ muscle fibers (Fig. 3 *B* and *D*). Even though $C2^{-/-}$ increases the expression of sMyBP-C (Fig. 1 *C* and *E*), it did not result in expansion of the spatial distribution of sMyBP-C in the sarcomere. Similarly, ultrastructural electron microscopy analyses revealed that sarcomeres remained well aligned in the absence of fMyBP-C (*SI Appendix*, Fig. S6). The widths of the A-band, Z-disk, and M lines were not significantly different between WT and $C2^{-/-}$ (*SI Appendix*, Table S5). Overall, $C2^{-/-}$ had no effect on gross sarcomere organization in EDL muscle. However, a significant increase in central nucleation (CN) and embryonic MHC (eMHC)-positive fibers was observed in $C2^{-/-}$ EDL cross sections (*SI Appendix*, Fig. S7). Since CN and eMHC are often indicators of muscle regeneration and/or degeneration, these findings show that KO of fMyBP-C may cause mild chronic muscle stress and/or damage in $C2^{-/-}$ EDL muscles.

fMyBP-C Modulates Mobility and Ordering of Myosin Heads. To determine the effect of fMyBP-C deletion on sarcomere dynamics, time-resolved small-angle X-ray diffraction images were collected every 20 ms from an intact EDL muscle during maximum isometric tetanic force generation (Fig. 4 *A* and *B*). The I_{11}/I_{10} intensity ratio is a measure of the relative degree of association between myosin heads and thin filaments. This ratio was an approximation of linear force over the period of activated tetanic force with the slope of this relationship being significantly greater in $C2^{-/-}$ as compared to WT (Fig. 4*C*), leading to a significantly increased I_{11}/I_{10} at peak force (Fig. 4*D*). The average change in I_{11}/I_{10} from rest to peak tetanic force generation ($\Delta I_{11}/I_{10}$) was twofold greater in $C2^{-/-}$ compared to WT EDL (2.79 versus 1.40, $P < 0.01$) (Fig. 4*E*). However, no difference was noted in I_{11}/I_{10} in the resting state (noncontracting) EDL muscles between the two

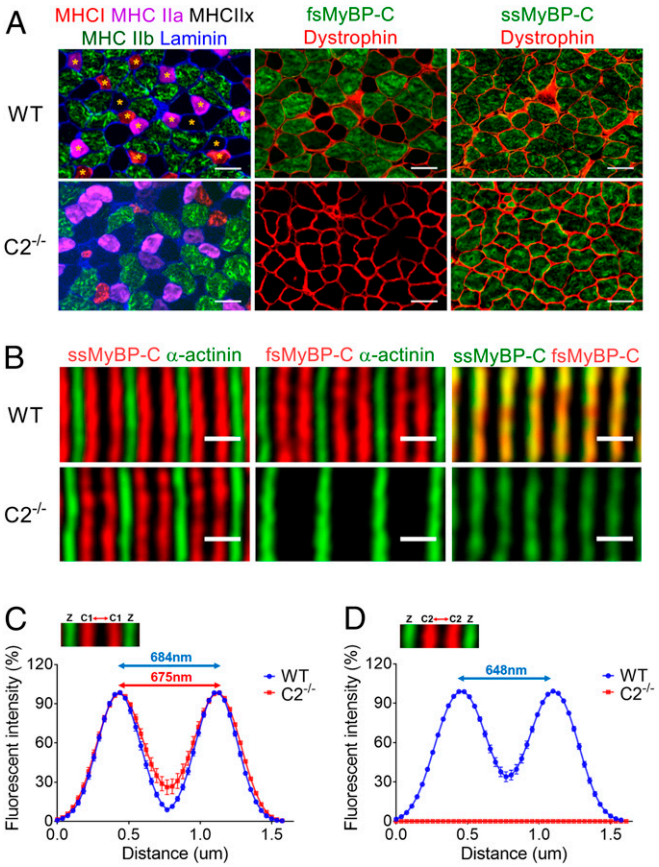

Fig. 3. Localization and spatial distribution of skeletal MyBP-C paralogs in EDL muscles. (*A*) Muscle fiber types were determined by expression of different MHC isoforms (*Left*). Global and equivalent protein expression of sMyBP-C in all WT and $C2^{-/-}$ fibers (*Right*). fMyBP-C protein was detected in large-sized fibers and colocalized with type IIb and some type IIx in WT (*Top*, *Middle*). Asterisks indicate fibers not expressing fMyBP-C. No type I or IIa fibers were colocalized with fMyBP-C (*Top*, *Left*). EDL muscles were serially sectioned at 10 μm thickness and stained with designated antibodies. (Scale bar: 50 μm.) (*B*) Skinned EDL fibers from WT and $C2^{-/-}$ were immmunostained with sMyBP-C, fMyBP-C, and α-actinin. A doublet pattern of sMyBP-C (red) between two Z-lines stained with α-actinin (green) (*Left*). fMyBP-C (red) was also detected in the same location and pattern as sMyBP-C in WT, but it was completely missing in $C2^{-/-}$ (*Middle*). (Scale bar: 1 μm.) The relative fluorescence signal of sMyBP-C and fMyBP-C, along with α-actinin, in skinned EDL fiber was measured from the images taken under high magnification (63×). The distribution of (*C*) sMyBP-C and (*D*) fMyBP-C fluorescence intensity was depicted in the graph. Two to three images were captured from one fiber, and two to three fibers were chosen from each mouse ($n = 3$). These values were the averaged distance between two peaks (*SI Appendix*, Fig. S5).

groups (Fig. 4*D*). The interfilament lattice was increased in $C2^{-/-}$ EDL compared to WT. This increase was significant in both intact (+0.8 nm, $P < 0.05$) and skinned EDL muscles (+1.5 nm, $P < 0.05$) (Fig. 4 *F* and *G*).

To examine the changes in myosin layer line, intensities in diffraction patterns during resting (Fig. 4*A*, left portion) and maximum isometric tetanic contraction (Fig. 4*A*, right portion) were measured. The intensity of the fourth myosin layer line (I_{MLL4}) under resting conditions was significantly lower in $C2^{-/-}$ compared to WT (Fig. 4*H*), indicating reduced quasi-helical ordering of the myosin heads around the thick filament backbone. However, the residual I_{MLL4} during isometric contraction (ratio of contracting I_{MLL4} over resting I_{MLL4}) was no different between the two genotypes, indicating that the relative changes in the proportion of ordered cross-bridges between rest and contraction were similar (*SI Appendix*, Fig. S8 *A* and *B*). In addition, fMyBP-C KO did not affect the movement of tropomyosin in the thin filaments during contraction (*SI Appendix*, Fig. S8*C*).

Ablation of fMyBP-C Results in Reduced Force Generation and Calcium Sensitivity in Single EDL Fibers. To further examine the contribution of fMyBP-C to lattice spacing and force generation in fast-twitch EDL muscle, we compared the contractility of skinned WT and $C2^{-/-}$ type IIb fibers treated with dextran (3% w:v). Dextran osmotically compresses the muscle and restores in vivo lattice spacing. $C2^{-/-}$ muscles produced significantly less steady-state isometric force both in the absence (Fig. 5*A*) and presence of dextran (Fig. 5*B* and *SI Appendix*, Table S6), and this reduction extended to lower concentrations of activating Ca^{2+}. At pCa 4.5, $C2^{-/-}$ muscles generated significantly less maximal force than that of WT (Fig. 5 *A* and *C* and *SI Appendix*, Table S6). Although dextran increased maximal force production for both WT and $C2^{-/-}$, $C2^{-/-}$ muscles still produced significantly less ($P < 0.01$) maximal steady-state isometric force (Fig. 5 *B* and *C* and *SI Appendix*, Table S6).

Myofilament calcium sensitivity (pCa_{50}) was significantly reduced in $C2^{-/-}$ compared to WT controls (Fig. 5*D* and *SI Appendix*, Fig. S9*A*). Although dextran increased pCa_{50} for both WT and $C2^{-/-}$, $C2^{-/-}$ still showed a statistically significant decrease in myofilament calcium sensitivity ($P < 0.01$) (Fig. 5*D* and *SI Appendix*, Fig. S9*B*). We then evaluated cross-bridge kinetics by measuring the rate of force redevelopment (k_{TR}) following a slack and restretch test. k_{TR} at maximal steady-state isometric activation (pCa 4.5) was comparable between groups (Fig. 5*E* and *SI Appendix*, Fig. S6). However, k_{TR} was significantly greater in $C2^{-/-}$ muscle at submaximal Ca^{2+} concentrations (pCa 5.5 to 5.2) compared to WT (Fig. 5*E*).

Compared to WT, $C2^{-/-}$ EDL muscles showed significantly less sinusoidal muscle stiffness at all levels of calcium activation in both the absence or presence of dextran (Fig. 5*F* and *SI Appendix*, Fig. S9*C*). Interestingly, restoration of in vivo lattice spacing with dextran resulted in a greater relative increase of force generation (Fig. 5*C*) and maximal sinusoidal stiffness (Fig. 5 *G* and *H*) in $C2^{-/-}$ EDL muscle compared to that in WT muscles. Rigor stiffness showed no significant differences between WT and $C2^{-/-}$ in the presence or absence of dextran (Fig. 5*H*). The ratio of maximal active stiffness to rigor stiffness can be used to measure the proportion of active force-producing cross-bridges (17). In $C2^{-/-}$ EDL muscle, this ratio is substantially reduced in both the absence (WT = 65% and $C2^{-/-}$ = 49%) and presence (WT = 60% and $C2^{-/-}$ = 51%) of dextran, indicating that $C2^{-/-}$ muscles have proportionately fewer force-producing cross-bridges during active contraction as compared to WT.

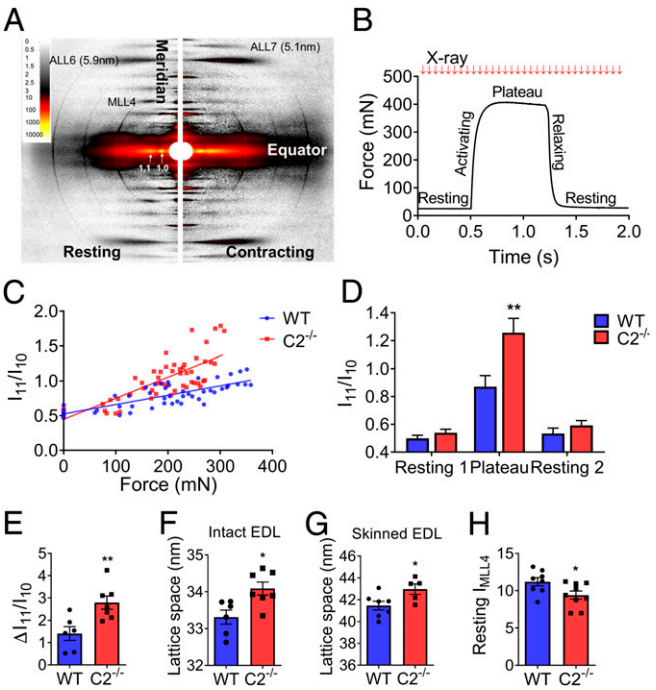

Fig. 4. Increased sarcomere lattice spacing and disorganized myosin movement in $C2^{-/-}$ EDL intact muscles and skinned fibers. (*A*, *Left*) X-ray diffraction pattern of EDL muscle at rest (*Right*) and during contraction. Equatorial reflections (I_{11} and I_{10}) and layer line patterns (MLL4, ALL6, and ALL7) are as indicated. (*B*) Force as a function of time during maximally activated isometric tetanus of EDL muscle. X-ray exposures (10 ms) were taken every 20 ms during isometric contraction. (*C*) Linear relationship of the ratio of I_{11} to I_{10} (I_{11}/I_{10}) to force development. Slope of I_{11}/I_{10}, as a function of force, is steeper in $C2^{-/-}$. (*D*) Average I_{11}/I_{10} during rest and maximal contraction. *X*-axis indicates resting (1 and 2) and plateau periods during the contraction as shown in Fig. 4*B*. (*E*) Change in I_{11}/I_{10} relative to rest during isometric muscle contraction. (*F*) Calculated lattice spacings in intact EDL muscle at optimal muscle length (L_o) (*G*) and skinned EDL fibers at sarcomere length 2.2 μm. (*H*) Intensity of MLL4 in resting EDL muscle ($n = 6$ to 9 in each group). Error bars represent ± SEM, $^*P < 0.05$ and $^{**}P < 0.01$. Statistical analyses were performed in all groups by unpaired *t* test or ordinary two-way ANOVA followed by Bonferroni's multiple comparison test.

Molecular Compensation from the Loss of fMyBP-C. Molecular compensatory responses of individual fast-twitch fibers in the absence of fMyBP-C were evaluated by single muscle fiber transcriptomic (RNA sequencing, or RNA-seq) analysis (18). In total, 191 differentially expressed genes (DEGs) were identified between $C2^{-/-}$ and WT fibers (*SI Appendix*, Fig. S10). Key genes which negatively regulate inflammatory responses (IFITM3 and CSF1) and actin filament polymerization (GSN, PALMD, and LMOD1) were identified among the 15 most deregulated genes in $C2^{-/-}$ fibers. Genes regulating muscle regeneration and differentiation (TMEM8C, PALMD, and APCDD1) were also significantly decreased, while negative regulators of muscle regeneration (PHLDA3 and METTL21C) were increased in $C2^{-/-}$ fiber (*SI Appendix*, Fig. S10*A*). Gene ontology enrichment analysis indicated that signaling pathways related to inflammatory responses, actin polymerization, and muscle regeneration/differentiation were significantly up-regulated in $C2^{-/-}$ samples (Fig. 6*A* and *SI Appendix*, Fig. S10*B*). Changes in the transcript levels of six different sMyBP-C variants were determined by RNA-seq in EDL fibers (*SI Appendix*, Fig. S11) and generally showed modest and variable differences in expression among isoforms in both WT and $C2^{-/-}$, likely accounting for the effects of fMyBP-C ablation on structure and contractility.

Next, we performed global proteomic and phosphoproteomics of WT and $C2^{-/-}$ EDL fibers (*SI Appendix*, Tables S7–S9) to examine whether compensatory changes in the expression, or post-translational modifications, of sarcomeric proteins could

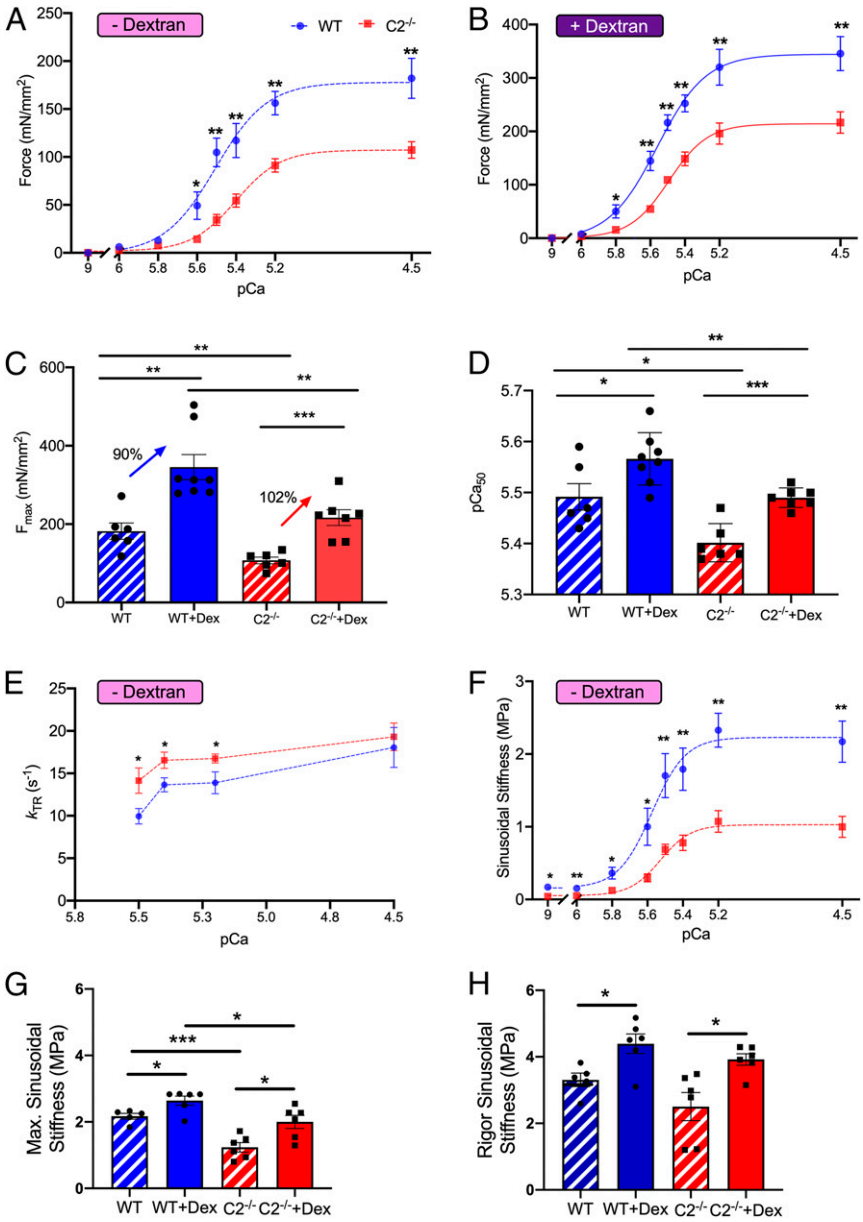

Fig. 5. Reduced maximal isometric force, calcium sensitivity of steady-state muscle activation, and sinusoidal stiffness in fast-twitch fiber of $C2^{-/-}$ EDL skinned fibers. (*A*) Force–pCa curve of skinned single EDL fiber in pCa 9.0 to 4.5 at 2.3 μm sarcomere length. (*B*) Increased steady-state isometric force generation after 3% dextran treatment in both WT and $C2^{-/-}$ muscle fiber. (*C*) Maximum isometric force at pCa 4.5 with or without dextran treatment. The increase of isometric maximal force in $C2^{-/-}$ fiber in dextran versus nondextran was 12% higher than that of WT in dextran versus nondextran. (*D*) Significantly decreased myofilament calcium sensitivity of contraction (pCa_{50}) in $C2^{-/-}$ fiber with and without dextran treatment. (*E*) k_{TR} in submaximum calcium concentrations (pCa 5.5 and 5.4) increased in $C2^{-/-}$($n = 6$ in each group) and (*F*) reduced sinusoidal stiffness of $C2^{-/-}$ fiber in all calcium concentrations (pCa 9.0 to 4.5). (*G*) Maximum sinusoidal stiffness at pCa 4.5 increased more in $C2^{-/-}$ (+62%) compared to WT (+22%) after dextran (3%) treatment (WT, $n = 5$ to 6 and $C2^{-/-}$, $n = 6$). (*H*) Complete deletion of fMyBP-C protein has no effect on sinusoidal stiffness during rigor in EDL muscle. (*A–F*) WT, $n = 6$; WT + Dex, $n = 8$; $C2^{-/-}$, $n = 6$; and $C2^{-/-}$ + Dex, $n = 7$. (*H*) WT, $n = 5$; WT + Dex, $n = 6$; $C2^{-/-}$, $n = 6$; and $C2^{-/-}$ + Dex, $n = 6$. Error bars represent ± SEM, $^*P < 0.05$, $^{**}P < 0.01$, and $^{***}P < 0.001$. NS, nonsignificant. Statistical analyses were performed in WT and $C2^{-/-}$ by unpaired Student's *t* test in each condition.

account for the functional changes seen in $C2^{-/-}$ muscle (19). In addition, we measured by Western blot the phosphorylation levels of sMyBP-C at the Ser-59/Ser-62 sites (20) and phosphorylation of myosin regulatory light chain 2 (MLC2) at the Ser-16 site (21). Despite an increase in total sMyBP-C expression, no difference was seen in sMyBP-C phosphorylation levels between WT and $C2^{-/-}$ (*SI Appendix*, Figs. S12 and S13). The total MLC2 protein was significantly decreased (−26%) with no change of MLC2 phosphorylation in $C2^{-/-}$ EDL intact muscles (*SI Appendix*, Fig. S13). Interestingly, expression of the skeletal muscle stress response proteins, ankyrin repeat domain containing protein 2 (*Ankrd2*) and crystallin αB (*Cryab*), increased in $C2^{-/-}$ EDL. Elevated levels of these proteins were further validated by Western blot analysis (*SI Appendix*, Fig. S14). Lastly, comparison of RNA-seq and mass spectroscopy data revealed DEGs and differentially translated proteins in $C2^{-/-}$ fibers in gene clusters related to muscle contraction, inflammation, actin filament polymerization, and muscle regeneration and differentiation (Fig. 6*A* and *SI Appendix*, Figs. S15 and S16).

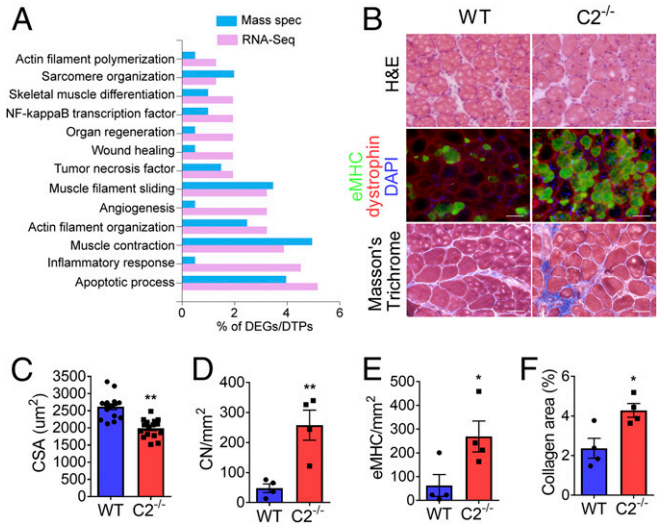

Fig. 6. Severe muscle damage in $C2^{-/-}$ after chronic mechanical overloading. (*A*) Bar plot showing specific gene ontology biological process and associated percentage of DEGs [cutoff: log2 fold change > 2; $P < 0.05$] and differentially translated proteins ($P < 0.05$) from RNA-seq and mass spectrometry, respectively, generated using the FunRich 3.1.3 tool. (*B*) Representative images of cross-sectioned PLN muscles at 14 d after synergistic muscle ablation-induced overloading. (*Top*) Samples were stained with hematoxylin and eosin and (*Bottom*) Masson's trichrome or (*Middle*) immunostained with antibodies against eMHC (green), dystrophin (red), and DAPI (blue). (*C*) Smaller cross-sectional area (CSA) of PLN muscle in $C2^{-/-}$. Average CSA of PLN muscle fiber was measured in four areas per muscle ($n = 4$ PLN per group). (*D*) Average number of CN- and (*E*) eMHC-positive fibers as well as (*F*) the fibrotic tissue area in PLN was increased in $C2^{-/-}$ after overloading. Three to four different areas in each section were examined and averaged in each muscle ($n = 4$ PLN per group). (Scale bar: 50 μm.) $^{*}P < 0.05$ and $^{**}P < 0.01$. Statistical analyses were performed in all groups by unpaired *t* test.

Maladaptation of $C2^{-/-}$ Muscle to Mechanical Overload. Fast skeletal muscles normally exhibit hypertrophy in response to chronic overload (21). We compared the response of WT and $C2^{-/-}$ plantaris muscles (PLN) to mechanical overload, which was generated by removing synergistic muscles (the SOL and 70% of the gastrocnemius). The $C2^{-/-}$ PLN was significantly less hypertrophied after 2 wk of overload compared to WT PLN (Fig. 6 *B* and *C*). In addition, the number of fibers containing CN increased significantly in $C2^{-/-}$ PLN (Fig. 6*D*). Similarly, $C2^{-/-}$ PLN exhibited an increased number of eMHC-positive fibers (Fig. 6*E*) and greater area occupied by fibrotic tissue (Fig. 6*F*) compared to WT. Altogether, these data demonstrate that expression of fMyBP-C is vital for regeneration and proper load-induced muscle growth.

Discussion

fMyBP-C Is Essential for Generating Maximal Force in Fast Skeletal Muscles. The fMyBP-C paralog is predominantly expressed in fast-twitch muscles, specifically within type IIb fibers, while sMyBP-C is expressed in both fast- and slow-twitch muscles (14). However, the physiological, structural, and functional roles of fMyBP-C in skeletal muscles are unknown. To define these roles, we used newly generated $C2^{-/-}$ mice in which fMyBP-C expression was globally ablated in all muscle types. Importantly, $C2^{-/-}$ was benign with no signs of excess morbidity and mortality. $C2^{-/-}$ EDL fibers, however, showed reduced contractility when stimulated both in vivo and ex vivo, and their hypertrophic response to mechanical overload was impaired. Furthermore, $C2^{-/-}$ EDL muscles contracted more slowly during isotonic contraction and generated lower maximal and submaximal forces during isometric contractions as compared to WT muscles. These findings imply that expression of fMyBP-C is critical for generating maximal force under resistance exercise, in which a greater number of cross-bridges are needed to match the increased force and power requirements. Such a role is consistent with the greater relative expression of fMyBP-C in fast-twitch (type IIb) fibers, which are activated when greater force, power output, and contraction speed are required (6). We can see parallels to these findings in zebrafish muscles, which lack fMyBP-C, correspondingly producing less maximum tetanic force (6). Similarly, 70% knockdown of sMyBP-C in mouse flexor digitorum brevis results in significantly decreased contractility and, hence, markedly reduced twitch and tetanic force and contraction velocity (22). In contrast, cMyBP-C KO results in enhanced force development (k_{TR}) with increasing actomyosin kinetics without changing maximal force (23). The deletion of cMyBP-C in cardiac muscle induced a similar inflammatory response, also suggesting abnormal regenerative processes (5, 24). Taken together, our studies demonstrate that fMyBP-C is essential for generating maximal force in fast-twitch muscle. These findings highlight the different regulatory roles of MyBP-C paralogs in different striated muscles when considering the fundamental aspects of muscle contraction, such as thin filament activation, calcium handling, and actomyosin interaction (9).

Compensatory Responses for the Loss of fMyBP-C in Fast Skeletal Muscles. In the present study, ablation of fMyBP-C in skeletal muscle induced an increase of greater than 30% in sMyBP-C expression without changing its phosphorylation status, suggesting that fMyBP-C and sMyBP-C transcomplementation may occur in the absence of one or the other in skeletal muscles. While sMyBP-C may partially compensate for the loss of fMyBP-C, functional data suggest that this compensation is insufficient to fully maintain the force of contraction and fully replace the function of fMyBP-C in fast-twitch muscle. We also determined that total MLC2 protein is down-regulated in $C2^{-/-}$ EDL muscles, most likely contributing to the observed reduction in force and speed of contraction (21). Significantly increased expression of *Ankrd2* and *Cryab* proteins can be attributed to the secondary effects of fMyBP-C deletion, indicating elevated muscle stress and damage in $C2^{-/-}$ EDL (25, 26). Finally, single-fiber RNA-seq data demonstrated that tumor necrosis factor–mediated signaling pathways, negative actin polymerization, and muscle regeneration/differentiation were all significantly up-regulated, suggesting additional responses compensating for the lack of fMyBP-C beyond those from sMyBP-C. Overall, compensatory sMyBP-C up-regulation, secondary consequences of MLC2 loss, and elevated *Ankrd2* and *Cryab* highlight the essential role of fMyBP-C in regulating maximal force and velocity of contraction under high mechanical loads in fast skeletal muscles. While it is beyond the scope of this paper, future work will undertake a systematic study using sMyBP-C, fMyBP-C, and double KO mouse models to define this compensatory activity in the context of muscle disease.

Ablation of fMyBP-C Results in Reduced Myofilament Calcium Sensitivity. In general, MyBP-C paralogs modulate actomyosin interactions via their N-terminal regions (C1 to C2 domains) (9). Similar to the cMyBP-C null phenotype (23), fMyBP-C null myofilaments showed decreased myofilament calcium sensitivity, indicating that more calcium is required to generate half-maximum force compared to controls. Previously, we reported that the amino terminal region of fMyBP-C increases force generation and calcium sensitivity while reducing sliding velocities at high Ca^{2+} (9). These results demonstrate that fMyBP-C functions in a manner similar to that of cMyBP-C but not sMyBP-C. Since the amino terminus is the region with greatest divergence among MyBP-C paralogs, fMyBP-C may have evolved to optimize faster force generation at levels of intracellular calcium required to meet the demand of fast-twitch fiber

contraction. Intracellular calcium in fast skeletal muscles operates over a wide dynamic range and is characterized by periods of steady nanomolar levels [Ca^{2+}] at rest punctuated by brief bursts of high (micromolar) levels of Ca^{2+} in active muscles. Conversely, sMyBP-C promotes thin filament activation at low Ca^{2+} concentration (9). By contrast, Ca^{2+} changes in cardiac muscle fluctuate over a wide range of concentrations in a continuously repeating cycle. Although fMyBP-C expression is normally undetectable in cardiac muscle, it is up-regulated in hypertrophied myocytes, which must produce force against greater loads (14). Thus, different MyBP-C paralogs appear to play distinct roles in thin filament activation and myofilament regulation in order to generate rates and force of contraction appropriate for the tissues in which they are found.

Increased Myofilament Lattice Spacing and Increased Mobility of Myosin Heads but Smaller Proportion of Force-Producing Cross-Bridges in $C2^{-/-}$ EDL Fibers. Compared to WT, X-ray diffraction analysis indicated that $C2^{-/-}$ EDL fibers had fewer myosin heads quasi-helically ordered around the thick filament backbone at rest and that a greater shift of mass takes place in the form of myosin heads toward actin during maximum isometric tetanic contraction. These differences occurred in association with a larger actomyosin lattice spacing in $C2^{-/-}$ muscle at rest. Computational modeling studies (27) indicate that increased lattice spacing, relative to in vivo spacing, results in less force per active cross-bridge, that is, cross-bridges become less efficient when the lattice is perturbed away from the in vivo spacing. This notion is supported by the stiffness data showing a substantial increase in the ratio of maximal active stiffness to rigor stiffness, a measure of the proportion of force-producing active cross-bridges in both $C2^{-/-}$ and WT in the presence of dextran where the in vivo spacing is restored (17). Larger lattice spacing by itself, therefore, can account for some fraction of the force deficit in $C2^{-/-}$ EDL muscle fibers. Based on our observations, we propose that fMyBP-C deletion causes dysregulation of thick filament-based activation mechanisms, increases lattice spacing, and decreases calcium sensitivity in a manner similar to that of the impact of null cMyBP-C on cardiac muscles (23, 28).

Changes in actomyosin interactions are consistent with the observed significant reduction in sinusoidal stiffness during steady-state muscle activation. Lattice spacing alone, however, is unlikely to account for the entire force deficit in $C2^{-/-}$ muscle. Our stiffness data indicate a substantially smaller fraction of force-producing cross-bridges in $C2^{-/-}$ compared to WT at all levels of calcium activation. $C2^{-/-}$ displayed significantly reduced maximal sinusoidal stiffness in both the absence and presence of dextran. Part of this decrease may result from the increased lattice spacing. Restoration of in vivo lattice spacing with dextran resulted in a proportionally greater increase of force generation in $C2^{-/-}$ muscle than that in WT. Finally, the ratio of maximal active stiffness to rigor stiffness is substantially reduced in $C2^{-/-}$ EDL muscle relative to WT in both the absence and presence of dextran. This is a clear indication that $C2^{-/-}$ has a lower proportion of force-producing cross-bridges during active contraction as compared to WT, regardless of the lattice spacing. This is likely to be the primary factor contributing to reduced force in the absence of fMyBP-C in skeletal muscle.

The lower proportion of force-producing cross-bridges could also be a result of fewer cross-bridges stereospecifically bound to actin or fewer bound cross-bridges able to efficiently produce force (27). We do not have enough information to resolve this question. Nonetheless, it is clear from the k_{TR}, myosin layer line, and I_{11}/I_{10} measurements that the deficit does not result from an inability of the heads to reach actin owing to helical ordering around the thick filament backbone; rather, the force deficit originates from altered actomyosin interactions per se.

We might ask how to reconcile the smaller fraction of force-producing cross-bridges with X-ray diffraction data indicating a greater proportion of myosin heads associated with the thin filament. Some evidence to address this question is provided by Brunello et al., who report that myosin heads in the so-called D-zones of cardiac muscle lack MyBP-C on the thick filaments (29). As such, these myosin heads are predominantly in a disordered relaxed state rather than quasi-helically arranged around the thick filament backbone, which is confined to the C-zone. This result suggests that the presence of fMyBP-C in the C-zone helps maintain the ordered arrangement in the super relaxed state. If so, a reduction in I_{MLL4} and an increase in I_{11}/I_{10} would be expected in $C2^{-/-}$ muscle because myosin heads are no longer held in an ordered array near the thin filament backbone via interactions with fMyBP-C. In fMyBP-C KO, the increased density of myosin heads near actin could form weaker and more transient interactions with the thin filament at high load as occurs within the C-zone, thereby attenuating the force and velocity of contraction.

An alternative hypothesis holds that fMyBP-C helps maintain myosin attachment and/or detachment during the large step-size required for high load contraction in fast muscles. This hypothesis is supported by the increased curvature of the force–velocity relationship and significantly reduced sinusoidal stiffness during steady-state muscle activation and rigor in $C2^{-/-}$ EDL muscles. While the underlying mechanisms remain unclear, the inability of $C2^{-/-}$ EDL muscles to contract normally against high loads results in pathological remodeling when chronically overloaded, as was observed. Collectively, these results suggest that fMyBP-C fine-tunes myofilament organization in a manner that supports more rapid activation and increases tolerance to mechanical overload. Conversely, the absence of fMyBP-C disrupts this organization and hinders force generation. In addition, the finding that rate of relaxation ($-dF/dt$) is reduced at all stimulation frequencies in EDL muscles of $C2^{-/-}$ mice suggests that fMyBP-C contributes to muscle relaxation. This impairment of relaxation is not unexpected, as similar observations have been made regarding the role of cMyBP-C in cardiac muscle relaxation (30).

fMyBP-C Null Muscles Respond Weakly to Mechanical Overload. Normally, mechanical overload on skeletal muscle induces hypertrophy and activates a compensatory program of repair and regeneration that replaces damaged fibers. These responses are impaired in the $C2^{-/-}$ mouse EDL, both under baseline conditions and after chronic overload. Even after modest mechanical loading consistent with daily life, $C2^{-/-}$ EDL muscles exhibited damage and ongoing repair/regeneration responses, and chronic overload greatly exacerbated these maladaptations. The overloading of $C2^{-/-}$ mouse plantaris muscle induced severe muscle damage and triggered an ongoing elevated regenerative response which, however, could not rescue the damage. In many regions, fibrotic tissue, rather than new adult muscle fibers, replaced damaged muscle. Furthermore, transcriptome analysis of single muscle fibers demonstrated activation of inflammatory and muscle degeneration pathways in the mice.

The failure to respond to mechanical overload may be directly related to the genetic deletion of fMyBP-C, or it may reflect a sensitization owing to preexisting deficits in the muscle function of $C2^{-/-}$ mice. While the evidence needed to resolve this question cannot be derived from the present data, we will consider it in future studies.

Conclusion

Collectively, our results indicate that fMyBP-C plays a foundational role in the proper regulation of contractile structure and function with distinct adaptations for fast skeletal muscles. fMyBP-C modulates actomyosin recruitment and cross-bridge interactions to match contractile output to demand, and this role is critical for maximal force generation. While some mechanistic questions remain to be addressed, notably, the link between force generation and molecular compensation in muscle,

the current study does provide key insights into the functional roles of myosin-binding proteins in the health and disease.

Materials and Methods

Generation of Global fMyBP-C KO Mouse Model. KO of the fMyBP-C was achieved by replacing exons 2 to 22 of the *Mybpc2* gene with a Neo cassette, and the KO mouse was genotyped as described in *SI Appendix*.

Steady-State Force Measurements. As previously described (31), in vivo grip strength, exercise capacity, and isometric tetanic torque of plantar flexion were measured. Ex vivo isometric force generation and isotonic speed of contraction in EDL and SOL muscle were also measured. Isometric force, sinusoidal stiffness, and force redevelopment (k_{TR}) of intact and chemically skinned single EDL fibers were measured at 2.3 μm sarcomere length in various calcium solutions ranging from pCa 9.0 to 4.5. See more details in *SI Appendix, Methods*.

Molecular Analyses. Gene and protein expressions were measured by single muscle fiber RNA sequencing, global proteomics and phosphomics, and Western blot analyses as described in *SI Appendix, Methods*. The mass spectrometry proteomics data have been deposited to the ProteomeXchange Consortium via the PRoteomics IDEntifications (PRIDE) partner repository with the dataset identifier PXD022316. RNA-seq data were deposited in the National Center for Biotechnology Information's (NCBI) Gene Expression Omnibus database (access no. GSE160827).

Immunofluorescence, Histology, and Electron Microscopy. Frozen sections and skinned EDL fibers ($n = 3$ to 4 in each group) were stained with hematoxylin and eosin and Masson's trichrome, immunostained with specific antibodies, and examined as previously described (31). To evaluate the integrity of sarcomere structure, fixed EDL muscles ($n = 3$ in each group) were cut and dehydrated. After embedding in Epon, samples were sectioned (at 70 nm thick) and stained with uranyl acetate followed by lead citrate (32). Grids were examined under a transmission electron microscope.

X-Ray Diffraction Analysis. X-ray diffraction pattern of EDL muscle was measured at rest and during isometric contraction as previously described (33). X-ray images were analyzed using the BioCAT MuscleX program suite (34).

Synergistic Muscle Ablation. Chronic mechanical overloading was induced in both plantaris muscles by surgically removing whole SOL and 70% of the gastrocnemius muscles. Adaptation to the overloading was evaluated histologically at 2 wk following surgery.

Statistical Analysis. All values presented as mean ± SE were compared with one- or two-way ANOVA with repeated measures, where appropriate, and the use of Bonferroni post hoc test to compare individual means.

Further experimental details are described in *SI Appendix*.

Data Availability. Proteomics and RNA-seq data have been deposited in PRIDE, NCBI's Gene Expression Omnibus (PXD022316; GSE160827).

ACKNOWLEDGMENTS. S.S. has received support from NIH grants R01 HL130356, R01 HL105826, R01 AR078001, and R01 HL143490 and American Heart Association 2019 Institutional Undergraduate Student (19UFEL34380251) and transformation (19TPA34830084) awards. T.S. (19POST34380448) and J.W.M. (17POST33630095) were supported with American Heart Association Fellowship training grants. R.C. was supported by NIH grants P01 HL059408, R01 AR067279, and R01 HL139883. This research used resources of the Advanced Photon Source, a US Department of Energy (DOE) Office of Science User Facility operated for the DOE Office of Science by Argonne National Laboratory under contract no. DE-AC02-06CH11357 and supported by grant P41 GM103622 from the National Institute of General Medical Sciences of the NIH. We thank Dr. Aikaterini Kontrogianni-Konstantopoulos for the sMyBP-C phospho-specific antibodies and Dr. Kwangmin Choi and Dr. Arif Mohammed for their support of RNA-seq and proteomics data analyses and interpretation. Through Loyola University Chicago, Dr. Pieter de Tombe provided institutional funding support to generate $C2^{-/-}$ mice. We thank the Proteomic and Metabolomics Facility of Cornell University for generating the mass spectrometry data and the funding support from the HHMI Transformative Technology 2019 Program for the Orbitrap Eclipse system.

1. R. Starr, G. Offer, Polypeptide chains of intermediate molecular weight in myosin preparations. *FEBS Lett.* **15**, 40–44 (1971).
2. M. Gautel, D. O. Fürst, A. Cocco, S. Schiaffino, Isoform transitions of the myosin binding protein C family in developing human and mouse muscles: Lack of isoform transcomplementation in cardiac muscle. *Circ. Res.* **82**, 124–129 (1998).
3. P. K. Luther *et al*., Understanding the organisation and role of myosin binding protein C in normal striated muscle by comparison with MyBP-C knockout cardiac muscle. *J. Mol. Biol.* **384**, 60–72 (2008).
4. E. Flashman, C. Redwood, J. Moolman-Smook, H. Watkins, Cardiac myosin binding protein C: Its role in physiology and disease. *Circ. Res.* **94**, 1279–1289 (2004).
5. B. K. McConnell *et al*., Dilated cardiomyopathy in homozygous myosin-binding protein-C mutant mice. *J. Clin. Invest.* **104**, 1235–1244 (1999).Corrected in: *J. Clin. Invest.* **104**, 1771 (1999).
6. M. Li, M. Andersson-Lendahl, T. Sejersen, A. Arner, Knockdown of fast skeletal myosin-binding protein C in zebrafish results in a severe skeletal myopathy. *J. Gen. Physiol.* **147**, 309–322 (2016).
7. D. Barefield *et al*., Haploinsufficiency of MYBPC3 exacerbates the development of hypertrophic cardiomyopathy in heterozygous mice. *J. Mol. Cell. Cardiol.* **79**, 234–243 (2015).
8. S. Sadayappan *et al*., Cardiac myosin-binding protein-C phosphorylation and cardiac function. *Circ. Res.* **97**, 1156–1163 (2005).
9. B. L. Lin *et al*., Skeletal myosin binding protein-C isoforms regulate thin filament activity in a Ca^{2+}-dependent manner. *Sci. Rep.* **8**, 2604 (2018).
10. C. A. Gurnett *et al*., Myosin binding protein C1: A novel gene for autosomal dominant distal arthrogryposis type 1. *Hum. Mol. Genet.* **19**, 1165–1173 (2010).
11. B. Markus *et al*., Autosomal recessive lethal congenital contractural syndrome type 4 (LCCS4) caused by a mutation in MYBPC1. *Hum. Mutat.* **33**, 1435–1438 (2012).
12. G. K. Dhoot, S. V. Perry, Expression of slow skeletal myosin binding C-protein in normal adult mammalian heart. *J. Muscle Res. Cell Motil.* **26**, 143–148 (2005).
13. M. A. Ackermann, A. Kontrogianni-Konstantopoulos, Myosin binding protein-C slow: A multifaceted family of proteins with a complex expression profile in fast and slow twitch skeletal muscles. *Front. Physiol.* **4**, 391 (2013).
14. B. Lin *et al*., Cardiac myosin binding protein-C plays no regulatory role in skeletal muscle structure and function. *PLoS One* **8**, e69671 (2013).
15. S. Cohen *et al*., During muscle atrophy, thick, but not thin, filament components are degraded by MuRF1-dependent ubiquitylation. *J. Cell Biol.* **185**, 1083–1095 (2009).
16. A. Li *et al*., Skeletal MyBP-C isoforms tune the molecular contractility of divergent skeletal muscle systems. *Proc. Natl. Acad. Sci. U.S.A.* **116**, 21882–21892 (2019).
17. M. Kawai, T. S. Karam, J. Kolb, L. Wang, H. L. Granzier, Nebulin increases thin filament stiffness and force per cross-bridge in slow-twitch soleus muscle fibers. *J. Gen. Physiol.* **150**, 1510–1522 (2018).
18. T. Song, S. Sadayappan, Fast skeletal myosin binding protein-C regulates fast skeletal muscle contraction *Gene Expression Omnibus* (GEO) database. https://www.ncbi.nlm.nih.gov/geo/query/acc.cgi?acc=GSE160827. Deposited 30 November 2020.
19. S. Zhang, Fast skeletal myosin binding protein-C regulates fast skeletal muscle contraction Proteomics IDEntification Database (PRIDE). https://www.ebi.ac.uk/pride/archive/projects/PXD022316. Deposited 3 November 2020.
20. M. A. Ackermann, C. W. Ward, C. Gurnett, A. Kontrogianni-Konstantopoulos, Myosin binding protein-C slow phosphorylation is altered in Duchenne dystrophy and arthrogryposis myopathy in fast-twitch skeletal muscles. *Sci. Rep.* **5**, 13235 (2015).
21. T. Kampourakis, Y. B. Sun, M. Irving, Myosin light chain phosphorylation enhances contraction of heart muscle via structural changes in both thick and thin filaments. *Proc. Natl. Acad. Sci. U.S.A.* **113**, E3039–E3047 (2016).
22. J. Geist, C. W. Ward, A. Kontrogianni-Konstantopoulos, Structure before function: Myosin binding protein-C slow is a structural protein with regulatory properties. *FASEB J.*, 10.1096/fj.201800624R (2018).
23. S. P. Harris *et al*., Hypertrophic cardiomyopathy in cardiac myosin binding protein-C knockout mice. *Circ. Res.* **90**, 594–601 (2002).
24. T. L. Lynch IV *et al*., Cardiac inflammation in genetic dilated cardiomyopathy caused by MYBPC3 mutation. *J. Mol. Cell. Cardiol.* **102**, 83–93 (2017).
25. M. A. Fortes *et al*., Overload-induced skeletal muscle hypertrophy is not impaired in STZ-diabetic rats. *Physiol. Rep.* **3**, e12457 (2015).
26. I. Dimauro, A. Antonioni, N. Mercatelli, D. Caporossi, The role of αB-crystallin in skeletal and cardiac muscle tissues. *Cell Stress Chaperones* **23**, 491–505 (2018).
27. S. Y. Bershitsky *et al*., Muscle force is generated by myosin heads stereospecifically attached to actin. *Nature* **388**, 186–190 (1997).
28. J. E. Stelzer, J. R. Patel, R. L. Moss, Protein kinase A-mediated acceleration of the stretch activation response in murine skinned myocardium is eliminated by ablation of cMyBP-C. *Circ. Res.* **99**, 884–890 (2006).
29. E. Brunello *et al*., Myosin filament-based regulation of the dynamics of contraction in heart muscle. *Proc. Natl. Acad. Sci. U.S.A.* **117**, 8177–8186 (2020).
30. C. N. Toepfer *et al*., Hypertrophic cardiomyopathy mutations in *MYBPC3* dysregulate myosin. *Sci. Transl. Med.* **11**, eaat1199 (2019).
31. T. Song *et al*., Dilated cardiomyopathy-mediated heart failure induces a unique skeletal muscle myopathy with inflammation. *Skelet. Muscle* **9**, 4 (2019).
32. E. S. Reynolds, The use of lead citrate at high pH as an electron-opaque stain in electron microscopy. *J. Cell Biol.* **17**, 208–212 (1963).
33. W. Ma, H. Gong, T. Irving, Myosin head configurations in resting and contracting murine skeletal muscle. *Int. J. Mol. Sci.* **19**, E2643 (2018).
34. J. Jiratrakanvong *et al*., MuscleX: Software Suite for Diffraction X-Ray Imaging V1.13.1 (Software copyright 1999 Illinois Institute of Technology, 2018), doi:10.5281/zenodo.1195050.